Reconfigurable Implication and Inhibition Boolean logic gates based on NAD$^+$-dependent enzymes: Application to signal-controlled biofuel cells and molecule release

Paolo Bollella[1,2] | **Vasantha Krishna Kadambar**[1] | **Artem Melman**[1] | **Evgeny Katz**[1]

[1] Department of Chemistry and Biomolecular Science, Clarkson University, Potsdam, New York, USA

[2] Dipartimento di Chimica, Università degli Studi di Bari "Aldo Moro", 70125 Bari, Italy

Correspondence
Prof. Paolo Bollella, Dipartimento di Chimica, Università degli Studi di Bari "Aldo Moro", 70125 Bari, Italy
Email: paolo.bollella@uniba.it

Prof. Artem Melman, Department of Chemistry and Biomolecular Science, Clarkson University, Potsdam, NY, 13699, USA
Email: amelman@clarkson.edu

Prof. Evgeny Katz, Department of Chemistry and Biomolecular Science, Clarkson University, Potsdam, NY, 13699, USA
Email: ekatz@clarkson.edu

Abstract

The Implication and Inhibition Boolean logic gates were realized using NAD$^+$/NADH-dependent dehydrogenases combined with hexokinase competing for biomolecule input signals. Both logic gates operated with the same enzyme composition and their reconfiguration was achieved simply by redefining the input signals. The output signals produced by the logic gates were analyzed optically and electrochemically, particularly using enzyme-modified electrodes. The logically processed input signals were used to switch operation of a biofuel cell and activate a molecule release process.

1 | INTRODUCTION

Molecule[1–3] and biomolecule[4] computing, particularly based on DNA/RNA-molecules[5,6] and enzyme-systems[7] have recently received high attention and have been studied extensively. While being a sub-area of unconventional computing,[8,9] the (bio)molecule computing systems are mostly considered for low-scale information processing expecting their applications in wearable[10] and implantable[11] bioelectronics, being particularly useful for signal-switchable/tunable (bio)sensors[12] and (bio)actuators,[13] for example, in biofuel cells with adaptable output controlled by logically processed molecule signals.[14] The advantage of the enzyme-based computing systems is their operation with metabolites signaling on various biochemical/biomedical changes.[15] While many biocomputing systems have been studied in a solution, following the binary (**0,1**) output signals optically, assembling these systems in an immobilized architecture, particularly at electrode interfaces, results in novel applications. Indeed, electrochemically readable outputs allow their use for triggering various actions. Particularly, the electrochemical logic systems can operate as binary (**Yes**/**No** or **1,0**) self-powered biosensors.[16] The present article demonstrates the extension of Boolean logic gates to signal-controlled actuators exemplified with biofuel cells and molecule-release systems.

2 of 9 | **Electrochemical Science Advances** | FULL ARTICLE
doi.org/10.1002/elsa.202100008

Chemistry
Europe
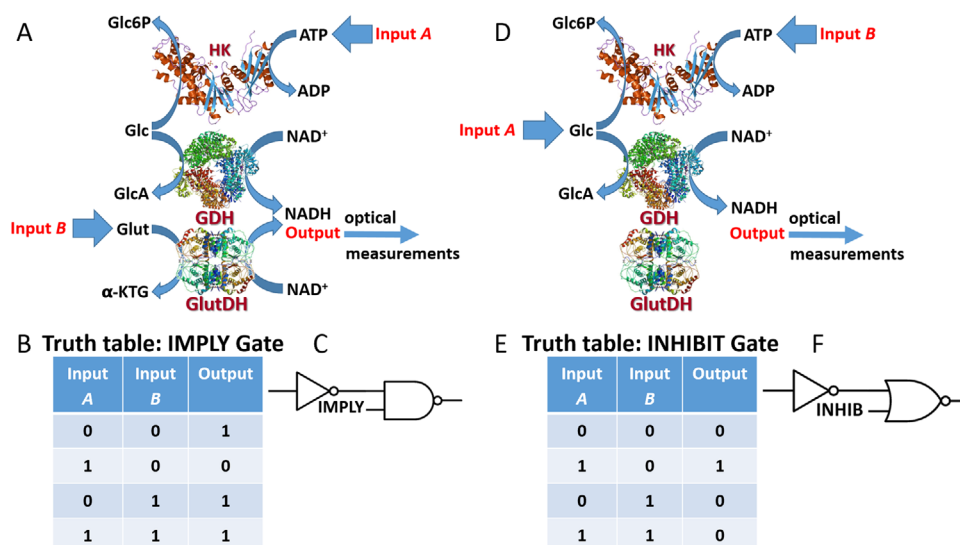European Chemical
Societies Publishing

FIGURE 1 (A and D) The schemes of the biocatalytic reactions used for mimicking the IMPLY and INHIB logic gates, respectively. (B and E) The truth tables of the IMPLY and INHIB Boolean logic gates, respectively. (C and F) The standard compositions of the IMPLY and INHIB gates, respectively, expressed in the conventional logic elements. The following abbreviations are used in the schemes: Glc6P – glucose-6-phosphate; GlcA – gluconic acid; α-KTG - α-ketoglutaric acid; ATP – adenosine 5′-triphosphate; ADP - adenosine 5′-diphosphate; other abbreviations are specified in the text

2 | RESULTS AND DISCUSSION

Enzyme-based systems have been used to mimic almost all Boolean logic operations, such as Yes, Not, OR, NOR, XOR, AND, NAND, etc.[17] While some of the logic gates particularly OR, AND gates, were studied in numerous versions for different applications, some other Boolean functions were modeled rarely. Particularly, Implication (IMPLY) logic operation, suggested more than a hundred years ago as an essential logic gate,[18] was understudied and its molecule realization has been reported only recently using various chemical (not bio-) systems[19–33] and in DNA-based systems,[34–45] particularly operating in cellular processes.[46] Enzyme-based systems mimicking the IMPLY logic gate have been reported only in very few recent papers.[16,47] A new realization of this gate with NAD$^+$/NADH-dependent enzymes allows high variability in the gate assembling due to a very broad selection of available enzymes operating according to the general concept applicable to all enzymes of the same family.

2.1 | Optical analysis of the logic gates operating in a solution

Figure 1A shows schematically the biocatalytic system for mimicking the IMPLY gate. The input signals for the binary operation of this gate were defined as the absence (logic value **0**) or presence in the experimentally optimized

concentration (logic value **1**) of the used chemicals: Input A (ATP: logic **0** – 0 mM; logic **1** – 1 mM), Input B (glutamate, Glut: logic **0** – 0 mM; logic **1** – 7.5 mM). Two input signals were applied in 4 different logic combinations: **0,0**; **1,0**; **0,1**; **1,1** (the first and second numbers correspond to Inputs A and B, respectively). All other chemicals: glucose dehydrogenase (GDH, EC 1.1.1.118, 1 U/mL), glutamate dehydrogenase (GlutDH, EC 1.4.1.3, 6 U/mL), hexokinase (HK, EC 2.7.1.1, 10 U/mL), glucose (Glc, 2 mM), and NAD$^+$ (0.8 mM) applied in an aqueous solution (see the exact composition in the Experimental Section) were used as a non-variable ("machinery") composition of the gate. The biocatalytically produced NADH, analyzed optically, corresponds to the Output **1**, while its absence (means the presence of the original non-reacted NAD$^+$) corresponds to the Output **0**. When the input signals are applied at **0,0** combination, the system generates Output **1** due to the reaction catalyzed by GDH (note that glucose is always present as a part of the "machinery"). Input combination **1,0** results in the Output **0**, because glucose is rapidly consumed in the reaction catalyzed by HK (note that HK has 10-fold higher activity than GDH), thus inhibiting the NADH production through the reaction catalyzed by GDH. On the other hand, input combination **0,1** produces Output **1**. Indeed, glucose is not consumed in the absence of ATP, then allowing NADH production in the reaction catalyzed by GDH. In addition, NADH is produced in the reaction catalyzed by GlutDH in the presence of glutamate. Thus, both biocatalytic reactions contribute to the NADH
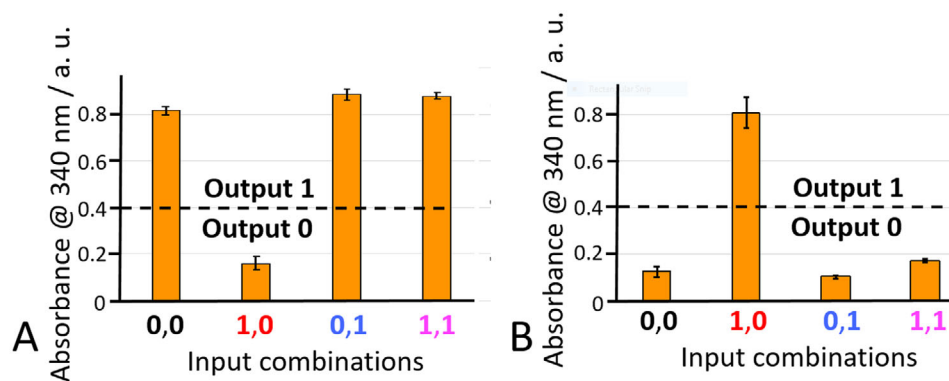
FIGURE 2 The bar-charts showing the output signals generated upon applying different input signal combinations to the system mimicking the IMPLY (A) and INHIB (B) logic gates. The bar charts show the average of 3 experiments for each input option with the relative standard deviations. The input signals and the background solution are specified in the Experimental Section

production yielding Output **1**. Finally, input combination **1,1** also results in Output **1**. While the reaction catalyzed by GDH is inhibited (note that glucose is consumed in the presence of ATP), another reaction catalyzed by GlutDH in the presence of glutamate results in the NADH production. The system performance corresponds to the truth table of the Boolean logic operation expected for the IMPLY gate (Figure 1B). Figure 1C shows a standard composition of the IMPLY gate expressed in the conventional logic elements. The optical analysis of the output signal produced in response to different input combinations is shown in Figure SI-9A (see in the Supporting Information, SI). The bar-chart (Figure 2A) derived from the experimental spectra shown in Figure SI-9A corresponds to the expected truth table of the IMPLY logic gate (Figure 1B).

The next studied Boolean operation was the Inhibition (INHIB) logic gate shown schematically in Figure 1D. Notably, the multi-enzyme biocatalytic system was exactly the same as one used for the realized IMPLY gate, but the input signals were redefined. Input *A* was defined as the absence (logic **0**) or presence (2 mM, logic **1**) of glucose. Then, glucose was excluded from the gate "machinery" composition. Input *B* was defined as the absence (logic **0**) or presence (1 mM, logic **1**) of ATP. Input combination **0,0** resulted in the Output **0** because the system lacks glucose as a substrate for GDH. Input combination **1,0** is the only one producing NADH (Output **1**) due to the reaction catalyzed by GDH in the presence of glucose and absence of ATP. Both input combinations **0,1** and **1,1** result in the Output **0** due to the absence of glucose (it is not added or it is consumed in the presence of ATP). In this system, GlutDH is not needed, but it was added for consistency to keep exactly the same gate composition for both logic operations. The system operation corresponds to the truth table for the INHIB Boolean logic gate, Figure 1E. Figure 1F shows a standard composition of the INHIB gate

expressed in the conventional logic elements. The optical analysis of the output signal produced in response to different input combinations is shown in Figure SI-9B (see in the SI). The bar-chart (Figure 2B) derived from the experimental spectra shown in Figure SI-9B corresponds to the expected truth table of the INHIB logic gate (Figure 1E). It is important to note that the INHIB logic gate produces exactly the opposite responses to the input signals comparing to the IMPLY gate, thus the INHIB gate can be considered as the negated IMPLY (Not-IMPLY) logic operation. Both operations can be performed with the same gate composition (at least in terms of the used enzymes), thus the transition from one gate to another can be just by re-definition of the input signals. Therefore, the developed approach allows the reconfigurable logic gates based on the same multi-enzyme system.

2.2 | Electrochemical analysis of the logic gates realized with enzymes immobilized at an electrode surface

While the optical analysis of the outcome signals generated by the enzyme system in a soluble state can be sufficient for demonstrating the system logic performance, immobilization of the enzymes at an electrode surface provides many advantages, particularly for connecting the logic gates to downstream bioelectronic devices activated with logically processed input signals. The GDH, GlutDH, and HK enzymes mimicking IMPLY and INHIB logic gates were immobilized at a buckypaper electrode (geometrical area ca. 1 cm^2) using 1-pyrenebutyric acid *N*-hydroxysuccinimide ester (PBSE) linker. The buckypaper electrode composed of compressed multi-walled carbon nanotubes (MWCNTs) has been frequently used for enzyme immobilization[48] and it is known for the
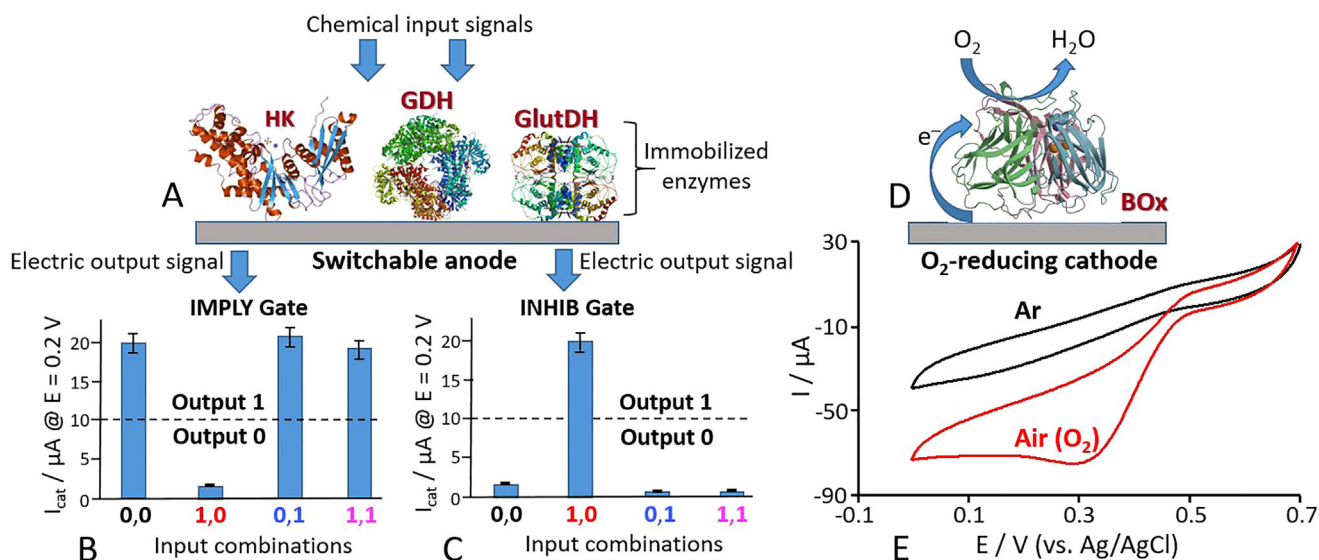
4 of 9   **Electrochemical Science Advances**   FULL ARTICLE
doi.org/10.1002/elsa.202100008

Chemistry
Europe
European Chemical
Societies Publishing

FIGURE 3 (A) Schematics of the enzyme-modified electrode logically processing input signals. (B and C) The bar-charts showing the electrocatalytic current output signals generated by the modified electrode upon applying different input signal combinations to the system mimicking the IMPLY (B) and INHIB (C) logic gates. The bar-charts show the average of three experiments for each input option with the relative standard deviations. The input signals and the background solution are specified in the Experimental Section. (D) Schematics of the oxygen-reducing BOx-modified electrode. (E) Cyclic voltammograms obtained for the BOx-modified electrode under Ar and air (in the presence of O_2). The potential scan rate, 2 mV/s

oxidation of NADH without the need of any additional catalysts.[49] The PBSE bifunctional linker strongly adsorbs at the buckypaper due to π–π staking of a highly aromatic pyrenyl group at sidewalls of MWCNTs, while the N-hydroxysuccinimide ester reacts with amino groups of enzyme lysine residues producing amide bonds,[50] (see Figure SI-1 in the SI). The surface load of the enzymes was estimated using standard assay procedures: GDH – 0.2 U/cm^2; GlutDH – 0.2 U/cm^2; HK – 1.5 U/cm^2 (see technical details and Figures SI-2, SI-3, SI-4 in the SI). Then, the enzyme-modified electrode was reacted with the input signals applied in four combinations: **0,0**; **1,0**; **0,1**; **1,1** (note that the definition of the input signals was different for the IMPLY and INHIB gates, as it was explained earlier). When the system responded to the input signals producing NADH (means Output **1**), the anodic currents corresponding to the NADH oxidation were observed (measured by cyclic voltammetry or chronoamperometry). Otherwise, when NADH is not produced (Output **0**), the currents were close to the background measured in the absence of the soluble components of the gate "machinery" (in a buffer solution only). The electrocatalytic current corresponding to the NADH oxidation was considered as the output signal generated by the logic gates (Figure 3A). The electrochemical responses for the IMPLY gate (Figure 3B) and for the INHIB gate (Figure 3C) correlate with the optically measured outputs (Figure 2) and correspond to the truth tables of the gates (Figures 1B,E).

2.3 | Extension of the logic gates to the downstream bioelectronic systems: A switchable biofuel cell and signal-triggered molecule release

In order to assemble a switchable biofuel cell, also used for a self-powered molecule release system, another buckypaper electrode was modified with bilirubin oxidase (BOx, EC 1.3.3.5, 1.1 U/cm^2, see Figures SI-5 and SI-6 in the SI). The BOx enzyme is frequently used as an O_2-reducing cathode in biofuel cells (Figure 3D).[51] The cyclic voltammogram obtained with the BOx-modified electrode (Figure 3E) demonstrates electrocatalytic O_2 reduction starting at the potential ca. 0.5 V. The NADH-oxidizing anode mimicking IMPLY and INHIB gates and O_2-reducing cathode were combined to operate as a biofuel cell. Figures 4A and 4B show polarization curves and power production dependence measured in two different states: (a) When the logic gates do not produce NADH (Output **0**) and (b) when the enzyme system generates NADH (Output **1**). Note that the active state of the biofuel cell can be obtained for different input signal combinations, depending on the logic gates realized (IMPLY or INHIB). The power produced by the switchable biofuel cell was considered as the output signal generated by the logic gates (Figure 4C,D) and the obtained results perfectly correlate with the optically measured outputs (Figure 2) and truth tables of the logic operations (Figure 1B,E).
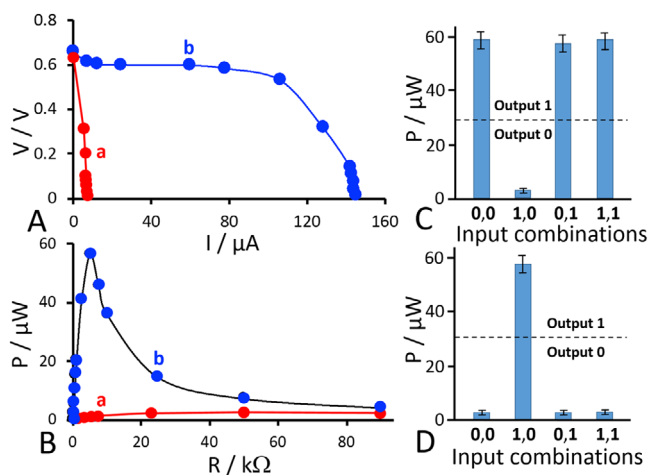
FIGURE 4 (A and B) The polarization function and power versus external load resistance, respectively, measured for the biofuel cell in the inactive (a) and active (b) states. The shown example functions were produced upon applying different input signal combinations, depending on the logic gates (IMPLY or INHIB). The biofuel cell was composed of the switchable GDH/GlutDH/HK-modified anode mimicking the logic gates and the BOx-cathode. (C and D) The bar-charts showing the output signals in the form of the power produced by the biofuel cell upon applying different input signal combinations to the systems mimicking the IMPLY and INHIB logic gates, respectively. The bar charts show the average of three experiments for each input option with the relative standard deviations. The input signals and the background solution are specified in the Experimental Section

In order to use the electrochemically realized logic gates for the signal-triggered molecule release, the BOx electrode was additionally modified with a fluorescent dye bound to the buckypaper support with a linker containing a chemical bond hydrolyzable at basic pH values (see Figure SI-5 in the SI). When the electrode is exposed to a solution with a basic bulk pH value, the unstable bond in the linker is hydrolyzed and the fluorescent dye is released to the solution (see Figure SI-7A in the SI). When the O_2 reduction catalyzed by the immobilized BOx proceeds, a local (interfacial) pH increases due to consumption of H^+ cations,[52] then the linker breaks apart and the dye is released. The O_2 reduction resulting in the dye release can be stimulated by applying potential from an external electronic instrument (potentiostat)[53] (see Figure SI-7B in the SI). When NADH is added to the solution, it can be oxidized at the buckypaper electrode, thus polarizing the electrode negatively and activating the O_2 reduction catalyzed by BOx. This process results in the local pH increase and the dye release (see Figure SI-8 in the SI). Finally, the O_2 reduction catalyzed by BOx can be activated upon operation of the biofuel cell composed by the switchable NADH-oxidizing electrode and the BOx-electrode contain-

ing the co-immobilized dye with the hydrolyzable linker. Indeed, the switchable electrode upon NADH oxidation provides electrons for the cathodic process at the BOx-electrode resulting in the local pH increase and the dye release. Since the electrochemical process is controlled by the IMPLY or INHIB logic gates, the dye release follows the same logic process (Figure 5). In other words, the output in the form of the dye release (Figures 5B and 5D for the IMPLY and INHIB gates, respectively) correlates with the output signals corresponding to the biofuel cell operation (Figures 4C and 4D), which in turn are based on the logic performance of the enzyme system measured primarily by optical means (Figure 2).

3 | CONCLUSIONS

In conclusion, the IMPLY and INHIB logic gates mimicked with the enzyme-catalyzed reactions were used to activate downstream bioelectronic systems producing electric power and then stimulating molecule release. The Boolean logic functions controlling the biofuel cell and release system can be easily changed from IMPLY to INHIB gate and back using the same enzyme composition only by re-defining the input signals. The released fluorescent dye was only an experimentally convenient substance, other (bio)molecule release in the signal-controlled fashion can be tailored for various applications. While the present study was only aimed at demonstrating how the reconfigurable logic gates can be used to control bioelectronic devices, the developed approach could lead to practically useful systems with signal-processing and self-powered operation. The designed systems provide conceptual promise for future biotechnological and biomedical operations in implantable[11] and wearable[10] bioelectronics.

4 | EXPERIMENTAL SECTION

4.1 | Chemicals and reagents

Enzymes : Glucose dehydrogenase (GDH, EC 1.1.1.118; from microorganism not specified by Toyobo Inc.), glutamate dehydrogenase from bovine liver (GlutDH, EC 1.4.1.3), hexokinase from *Saccharomyces cerevisiae* (HK, EC 2.7.1.1), bilirubin oxidase from *Myrothecium verrucaria* (BOx, EC 1.3.3.5), and glucose-6-phosphate dehydrogenase from Baker's yeast (*S. cerevisiae*) (G6PDH, EC 1.1.1.49).

Substrates/Co-substrates : Glucose (Glc), sodium L-glutamate (Glut), β-nicotinamide adenine dinucleotide, disodium salt hydrate reduced form (NADH),
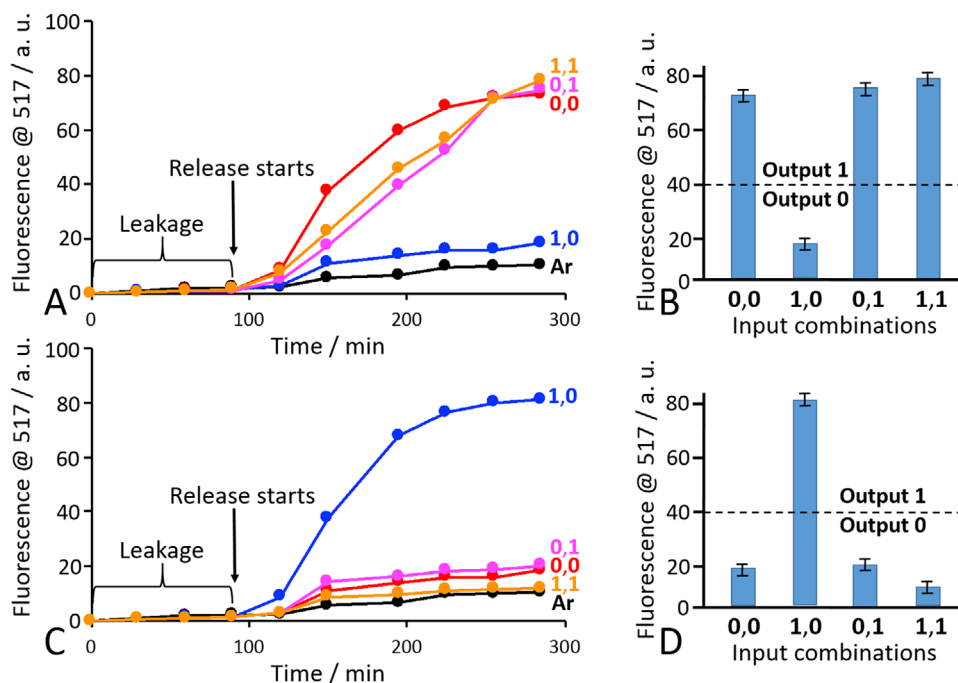
FIGURE 5 (A and C) The kinetics of the fluorescent dye release from the BOx-modified electrode with the co-immobilized dye bound to the electrode with a hydrolyzable linker. The curves correspond to the dye release by the systems mimicking the IMPLY (A) and INHIB (C) gates upon application of different input signal combinations. (B and D) The bar-charts showing the fluorescence of the released dye measured in the solution upon applying different input signal combinations to the system mimicking the IMPLY and INHIB logic gates, respectively. The bar-charts show the average of three experiments for each input option with the relative standard deviations. The input signals and the background solution are specified in the Experimental Section

β-nicotinamide adenine dinucleotide disodium salt hydrate oxidized form (NAD$^+$), adenosine 5′-triphosphate disodium salt hydrate (ATP), and 2,2′-azino-*bis*(3-ethylbenzothiazoline-6-sulphonic acid) (ABTS).

Buffers and solvents : tris(Hydroxymethyl)aminomethane (TRIS-buffer), 4-(2-hydroxyethyl)-1-piperazineethanesulfonic acid (HEPES-buffer), dimethyl sulfoxide (DMSO), isopropyl alcohol.

Other chemicals : 1-pyrenebutyric acid *N*-hydroxysuccinimide ester (PBSE), magnesium acetate (Mg(CH$_3$COO)$_2$), sodium sulfate (Na$_2$SO$_4$), and other standard chemicals and reactants.

All chemicals and reactants were purchased from MilliporeSigma (formerly Sigma–Aldrich; St. Louis, MO, USA), Alfa Aesar (Haverhill, MA, USA), AnaSpec Inc. (Fremont, CA, USA), and Toyobo Inc. (New York, NY, USA), and used without further purification.

Synthesis of the fluorescent dye with a hydrolyzable linker is detailed elsewhere.[54]

MWCNT buckypaper (high conductivity MWNT blend buckypaper, areal weight: 20 g/m^2) was purchased from NanoTechLabs Inc. (Yadkinville, NC, USA). All experiments were carried out in ultrapure water (18.2 MΩ·cm; Barnstead NANOpure Diamond).

4.2 | Instrumentation

A Shimadzu UV-2450 UV-Vis spectrophotometer with 1 mL (10 mm optical path) poly(methyl methacrylate) (PMMA) cuvettes was used for optical absorbance measurements. The fluorescence measurements were performed with an excitation wavelength of 490 nm and emission wavelengths 500–600 nm using a fluorescent spectrophotometer (Varian, Cary Eclipse). Electrochemical experiments were performed using an electrochemical workstation (ECO Chemie Autolab PASTAT 10) and GPES 4.9 (General Purpose Electrochemical System) software. All potentials were measured using a Metrohm Ag|AgCl|KCl, 3 M, reference electrode and a graphite slab was used as the counter electrode. All measurements were performed at room temperature, 20 ± 2 °C.

4.3 | The IMPLY logic gate operation in a solution with optical analysis of the output signals

All experiments were performed in 1 mL TRIS-buffer solution (3 mM, pH 7.0) containing 100 mM Na$_2$SO$_4$ and

20 mM $Mg(CH_3COO)_2$. The non-variable ("machinery") system was always present in the solution: HK (10 U/mL), GDH (1 U/mL), GlutDH (6 U/mL), NAD^+ (0.8 mM), and glucose (2 mM). The input signals were defined as:

> Input A (ATP): logic **0** – 0 mM (complete absence);
>   logic **1** – 1 mM
> Input B (Glut): logic **0** – 0 mM (complete absence);
>   logic **1** – 7.5 mM

The inputs were applied in 4 combinations: **0,0**; **1,0**; **0,1**; **1,1**. The input-chemicals were incubated with the "machinery" system for 7 minutes in the dark. The incubation time was optimized experimentally to allow the biocatalytic process to proceed to the end. The optical absorbance was measured recording UV-Vis spectra between $\lambda = 290$ nm and $\lambda = 410$ nm (characteristic range to observe the NADH reduced form). The initial absorbance spectra (measured prior to the input signals application) were subtracted from the final spectra recorded after 7 min of the reaction. The resulting differential spectra are shown in Figure SI-9A. The absorbance change measured at $\lambda_{max} = 340$ nm was defined as the output signals shown in Figure 2A.

4.4 | The INHIB logic gate operation in a solution with optical analysis of the output signals

The INHIB logic gate was realized similarly to the operation of the IMPLY gate with the following difference: glucose was not included in the "machinery" system and the input signals were redefined as:

> Input A (glucose): logic **0** – 0 mM (complete absence);
>   logic **1** – 2 mM
> Input B (ATP): logic **0** – 0 mM (complete absence);
>   logic **1** – 1 mM

The resulting differential spectra are shown in Figure SI-9B. The absorbance change measured at $\lambda_{max} = 340$ nm was defined as the output signals shown in Figure 2B.

4.5 | Preparation of the switchable enzyme-modified electrode

The buckypaper electrode (ca. 1 cm² geometrical area) was first incubated for 15 minutes in isopropyl alcohol and then thoroughly rinsed (3 times) with a working buffer solution (3 mM TRIS-buffer, pH 7.0, containing 100 mM Na_2SO_4 and 20 mM $Mg(CH_3COO)_2$). Then, a 20 μL solution containing 10 mM PBSE in DMSO was drop cast on

the electrode surface. Then, the electrode was carefully rinsed 2 times with DMSO and then rinsed with 3 mM HEPES-buffer, pH 6.0. Next, the electrode was incubated for 1 h at dark in a mixture containing 50 units of HK, 5 units of GDH, and 10 units of GlutDH (prepared in 25 mM HEPES-buffer pH 7.2). GlutDH is included also in the INHIBIT gate for consistency of the gate "machinery". Finally, the enzyme-modified electrode was rinsed with 3 mM TRIS-buffer, pH 7.0, containing 100 mM Na_2SO_4 and 20 mM $Mg(CH_3COO)_2$ and used in the electrochemical and signal-stimulated release experiments. Figure SI-1 shows the enzyme immobilization process schematically. The enzyme load on the modified electrodes was characterized by the standard enzyme-assay (see Figures SI-2, SI-3, SI-4 and SI-6 in the SI).

4.6 | Electrochemical measurements

The enzyme-modified electrode mimicking the IMPLY logic gate was characterized by measuring electrocatalytic current defined as the difference between the current produced in the presence of the input signals applied in 4 different combinations and the background current in the presence of the buffer only. The experiments were performed in 3 mM TRIS-buffer, pH 7.0, containing 100 mM Na_2SO_4 and 20 mM $Mg(CH_3COO)_2$ considered as starting buffer solution. In all experiments mimicking the logic gate operation 2 mM glucose and 0.8 mM NAD^+ were always present as a part of the gate "machinery." Input signals were applied in 4 different combinations: **0,0**; **1,0**; **0,1**; **1,1**. The input signals were defined as:

> Input A (ATP): logic **0** – 0 mM (complete absence);
>   logic **1** – 1 mM
> Input B (Glut): logic **0** – 0 mM (complete absence);
>   logic **1** – 7.5 mM

After 7 min of incubation with the input signals, the anodic currents were measured by cyclic voltammetry or chronoamperometry. The resulting catalytic current was considered as the output signal generated by the biocatalytic system.

The electrochemical study of the enzyme-modified electrode mimicking the INHIB was performed in the same way with the following difference: glucose was excluded from the "machinery" composition (it became an input signal) and the input signals were defined as:

> Input A (Glucose, Glc): logic **0** – 0 mM (complete absence); logic **1** – 2 mM
> Input B (ATP): logic **0** – 0 mM (complete absence);
>   logic **1** – 1 mM

8 of 9   **Electrochemical Science Advances**

FULL ARTICLE
doi.org/10.1002/elsa.202100008

Chemistry Europe
European Chemical
Societies Publishing

In the polarization experiments, either the IMPLY gate-anode or the INHIBIT gate-anode were connected with the BOx-modified electrode (containing also the dye-linker). The biofuel cell was tested in the presence of different input combinations. The voltage and current generated by the biofuel cell were measured with a multimeter (Meterman 37XR) with a variable resistance used as an external load. At every resistance, the system was let to equilibrate for 20 min in order to discard any possible contribution from a capacitive current. All measurements were performed at room temperature.

4.7 | Release experiments

Preparation of the electrode modified with BOx and a co-immobilized dye with a hydrolizable linker is detailed in the Supporting Information. The experiments were performed in 5 mL TRIS-buffer (3 mM, pH 7.0) containing 100 mM Na_2SO_4 and 20 mM $Mg(CH_3COO)_2$ considered as a starting buffer. After 90 min of equilibration to the solution (leakage process), the release was started by applying stimulating signals. In the major experiments the releasing electrode was connected to the switchable enzyme-modified electrode mimicking either IMPLY or INHIB logic gates processing input signals applied in 4 different combinations: **0,0; 1,0; 0,1; 1,1**. In additional (control) experiments (see Figures SI-7 and SI-8), the release was stimulated by changing the bulk pH value, applying potential from a potentiostat or adding NADH to the bulk solution.

CONFLICT OF INTEREST
The authors declare no conflict of interest.

DATA AVAILABILITY STATEMENT
The data that support the findings of this study are available from the corresponding author upon reasonable request.

REFERENCES
1. A.P. de Silva, *Molecular logic-based computation*, Royal Society of Chemistry, Cambridge, **2013**.
2. E. Katz (Ed.), *Molecular and supramolecular information processing – from molecular switches to logic systems*, Willey-VCH, Weinheim, **2012**.
3. K. Szacilowski, Infochemistry – information processing at the nanoscale, Wiley, Chichester, **2012**.
4. E. Katz (Ed.), *Biomolecular computing – from logic systems to smart sensors and actuators*, Willey-VCH, Weinheim, **2012**.
5. E. Katz (Ed.), *DNA- and RNA-based computing systems*, Wiley-VCH, Weinheim, **2021**.
6. Z. Ezziane, *Nanotechnology* **2006**, *17*, R27.
7. E. Katz, *Enzyme-Based Computing Systems*, Wiley-VCH, Weinheim, **2019**.
8. C.S. Calude, J.F. Costa, N. Dershowitz, E. Freire, G. Rozenberg (Eds.), *Unconventional Computation, Lecture Notes in Computer Science*, vol. *5715*, Springer, Berlin, **2009**.
9. A. Adamatzky (Ed.), *Advances in Unconventional Computing, in series: Emergence, Complexity and Computation*, Springer, Switzerland, **2017**.
10. O. Parlak, A. Salleo, A. Turner (Eds.), *Wearable Bioelectronics*, Elsevier, Amsterdam, **2020**.
11. E. Katz (Ed.), *Implantable Bioelectronics - Devices, Materials and Applications*, Wiley-VCH, Weinheim, **2014**.
12. E. Katz, J. Wang, M. Privman, J. Halámek, *Anal. Chem.* **2012**, *84*, 5463.
13. E. Katz, J. M. Pingarrón, S. Mailloux, N. Guz, M. Gamella, G. Melman, A. Melman. *J. Phys. Chem. Lett.* **2015**, *6*, 1340.
14. E. Katz, M. Pita, *Chem. Eur. J.* **2009**, *15*, 12554.
15. J. Halámek, J. R. Windmiller, J. Zhou, M.-C. Chuang, P. Santhosh, G. Strack, M. A. Arugula, S. Chinnapareddy, V. Bocharova, J. Wang, E. Katz, *Analyst* **2010**, *135*, 2249.
16. P. Bollella, Z. Guo, S. Edwardraja, V. Krishna Kadambar, K. Alexandrov, A. Melman, E. Katz, *Bioelectrochemistry* **2021**, *138*, 107735.
17. E. Katz, *ChemPhysChem* **2019**, *20*, 9.
18. A. Whitehead, B. Russell, *Principia Mathematica*. University Press, Cambridge, **1910**.
19. B. Tharmalingam, M. Mathivanan, B. Murugesapandian, *Spectrochimica Acta A* **2020**, *242*, 118749.
20. Q.-Q. Fu, J.-H. Hu, Y. Yao, Z.-Y. Yin, K. Gui, N. Xu, L.-Y. Niu, Y.-Q. Zhang, *J. Photochem. Photobiol. A* **2020**, *391*, 112358.
21. V. K. Singh, V. Singh, P. K. Yadav, S. Chandra, D. Bano, B. Koch, M. Talat, S. H. Hasan, *J. Photochem. Photobiol. A* **2019**, *384*, 112042.
22. S. Liao, X. Li, H. Yang, X. Chen, *Talanta* **2019**, *194*, 554.
23. Y.-M. Zhang, W. Zhu, W.-J. Qu, H.-L. Zhang, Q. Huang, H. Yao, T.-B. Wei, Q. Lin, *J. Luminescence* **2018**, *202*, 225.
24. L. Tang, S. Mo, S. G. Liu, L. L. Liao, N. B. Li, H. Q. Luo, *Sens. Actuat. B* **2018**, *255*, 754.
25. K. D. Renuka, C. L. Lekshmi, K. Joseph, S. Mahesh, *Chem. Select.* **2017**, *2*, 11615.
26. S. G. Liu, N. Li, Y. Z. Fan, N. B. Li, H. Q. Luo, *Sens. Actuat. B* **2017**, *243*, 634.
27. W.-T. Li, G.-Y. Wu, W.-J. Qu, Q. Li, J.-C. Lou, Q. Lin, H. Yao, Y.-M. Zhang, T.-B. Wei, *Sens. Actuat. B* **2017**, *239*, 671.
28. G. Wang, H. Chen, Y. Chen, N. Fu, *Sens. Actuat. B* **2016**, *233*, 550.
29. T. Liu, N. Li, J. X. Dong, H. Q. Luo, N.B. Li, *Sens. Actuat. B* **2016**, *231*, 147.
30. G. Singh, J. Singh, J. Singh, S. S. Mangat, *J. Luminescence* **2015**, *165*, 123.
31. A. Kuwar, R. Patil, A. Singh, S. K. Sahoo, J. Marek, N. Singh, *J. Mater. Chem. C* **2015**, *3*, 453.
32. J. Wu, Y. Gao, J. Lu, J. Hu, Y. Ju, *Sens. Actuat. B* **2015**, *206*, 516.
33. X. Tian, Z. Dong, J. Hou, R. Wang, J. Ma, *J. Luminescence* **2014**, *145*, 459.
34. X. Lin, Z. Hao, H. Wu, M. Zhao, X. Gao, S. Wang, Y. Liu, *Microchim. Acta* **2019**, *186*, 648.

9 of 9 **Electrochemical Science Advances**

FULL ARTICLE
doi.org/10.1002/elsa.202100008

Chemistry Europe
European Chemical
Societies Publishing

35. S. Ma, Q. Zhang, D. Wu, Y. Hu, D. Hu, Z. Guo, S. Wang, Q. Liu, J. Peng, *J. Electroanal. Chem.* **2019**, *847*, 113144.

36. J. Chen, J. Pan, S. Chen, *Chem. Sci.* **2018**, *9*, 300.

37. Y.-C. Chen, C. W. Wang, J. D. Lee, P.-C. Chen, H.-T. Chang, *J. Chinese Chem. Soc.* **2017**, *64*, 8.

38. Y.-F. Huo, L.-N. Zhu, X.-Y. Li, G.-M. Han, D.-M. Kong, *Sens. Actuat. B* **2016**, *237*, 179.

39. L. Ge, W. Wang, X. Sun, T. Hou, F. Li, *Anal. Chem.* **2016**, *88*, 9691.

40. X.-Y. Li, J. Huang, H.-X. Jiang, Y.-C. Du, G.-M. Han, D.-M. Kong, *RSC Adv.* **2016**, *6*, 38315.

41. R.-R. Gao, S. Shi, Y. Zhu, H.-L. Huang, T.-M. Yao, *Chem. Sci.* **2016**, *7*, 1853.

42. W. Gao, L. Zhang, R.-P. Liang, J.-D. Qiu, *Chem. – Eur. J.* **2015**, *21*, 15272.

43. Y. Jiang, N. Liu, W. Guo, F. Xia, L. Jiang, *J. Am. Chem. Soc.* **2012**, *134*, 15395.

44. K. S. Park, M. W. Seo, C. Jung, J. Y. Lee, H. G. Park, *Small* **2012**, *8*, 2203.

45. J.-H. Guo, D.-M. Kong, H.-X. Shen, *Biosens. Bioelectron.* **2010**, *26*, 327.

46. T. Miyamoto, S. Razavi, R. DeRose, T. Inoue, *ACS Synth Biol.* **2013**, *2*, 72.

47. K. Kaniewska, P. Bollella, E. Katz, *ChemPhysChem* **2020**, *21*, 2150.

48. A. J. Gross, M. Holzinger, S. Cosnier, *Energy Environ. Sci.* **2018**, *11*, 1670.

49. N. Lalaoui, N. Means, C. Walgama, A. Le Goff, M. Holzinger, S. Krishnan, S. Cosnier, *ChemElectroChem* **2016**, *3*, 2058.

50. V. A. Karachevtsev, S. G. Stepanian, A. Y. Glamazda, M. V. Karachevtsev, V. V. Eremenko, O. S. Lytvyn, L. Adamowicz, *J. Phys. Chem. C* **2011**, *115*, 21072.

51. F. Durand, C. H. Kjaergaard, E. Suraniti, S. Gounel, R. G. Hadt, E. Solomon, N. Manoa, *Biosens. Bioelectron.* **2012**, *35*, 140.

52. P. Bollella, A. Melman, E. Katz, *ChemElectroChem* **2020**, *7*, 3386.

53. M. Bellare, V. Krishna Kadambar, P. Bollella, E. Katz, A. Melman, *ChemElectroChem* **2020**, *7*, 59.

54. M. Bellare, V. Krishna Kadambar, P. Bollella, E. Katz, A. Melman, *Chem. Commun.* **2019**, *55*, 7856.

SUPPORTING INFORMATION

Additional supporting information may be found online in the Supporting Information section at the end of the article.